Article

Pyridinium salt-based covalent organic framework with well-defined nanochannels for efficient and selective capture of aqueous $^{99}TcO_4^-$

Mengjie Hao [a], Zhongshan Chen [a], Hui Yang [a,*], Geoffrey I. N. Waterhouse [b], Shengqian Ma [c,*], Xiangke Wang [a,*]

[a] College of Environmental Science and Engineering, North China Electric Power University, Beijing 102206, China
[b] MacDiarmid Institute for Advanced Materials and Nanotechnology, School of Chemical Sciences, The University of Auckland, Auckland 1142, New Zealand
[c] Department of Chemistry, University of North Texas, Denton, TX 76201, USA

A B S T R A C T

Ionic covalent organic framework (COF) materials with high specific surface areas and well-defined pore structures are desired for many applications yet seldom reported. Herein, we report a cationic pyridinium salt-based COF (PS-COF-1) with a Brunauer-Emmett-Teller (BET) surface area of 2703 m^2 g^{-1}, state-of-the-art for an ionic COF. Aided by its ordered pore structure, chemical stability, and radiation resistance, PS-COF-1 showed exceptional adsorption properties toward aqueous ReO$_4^-$ (1262 mg g^{-1}) and ^{99}TcO$_4^-$. Its adsorption performance surpassed its corresponding amorphous analogue. Importantly, PS-COF-1 exhibited fast adsorption kinetics, high adsorption capacities, and selectivity for ^{99}TcO$_4^-$ and ReO$_4^-$ at high ionic strengths, leading to the successful removal of ^{99}TcO$_4^-$ under conditions relevant to low-activity waste streams at US legacy Hanford nuclear sites. In addition, PS-COF-1 can rapidly decontaminate ReO$_4^-$/^{99}TcO$_4^-$ polluted potable water (~10 ppb) to drinking water level (0 ppb, part per billion) within 10 min. Density functional theory (DFT) calculations revealed PS-COF-1 has a strong affinity for ReO$_4^-$ and ^{99}TcO$_4^-$, thereby favoring adsorption of these low charge density anions over other common anions (e.g., Cl$^-$, NO$_3^-$, SO$_4^{2-}$, CO$_3^{2-}$). Our work demonstrates a novel cationic COF sorbent for selective radionuclide capture and legacy nuclear waste management.

© 2022 Science China Press. Published by Elsevier B.V. and Science China Press. All rights reserved.

1. Introduction

As a low-carbon emission technology, nuclear energy is expected to play an important role in satisfying the energy needs of future societies [1–3]. However, nuclear fission power plants generate spent nuclear fuels and radionuclide-containing wastes, which require careful management due to their extreme and persistent toxicity [4–6]. If intentionally or accidentally released into the environment, these radionuclides can accumulate in significant levels in groundwater [7–12], thereby posing significant long-term risk to humans, whilst being very difficult and expensive to remediate.

Technetium (^{99}Tc) is a radionuclide produced by the fission of ^{235}U or ^{239}Pu [4,13–15]. In water, it mainly exists as the pertechnetate ion (^{99}TcO$_4^-$), representing one of the most important radioactive anion hazards. Characteristics of ^{99}TcO$_4^-$ include a very high water solubility (11.3 mol L^{-1}), high toxicity due to beta particle emission, a long half-life (211,000 years), and extremely high mobil-

ity, thus making it difficult to selectively separate and remove from the nuclear waste and the environment [4,13–15]. Leaking of ^{99}TcO$_4^-$ from nuclear wastes into groundwater, leading to water contamination, results in concentration of the radionuclide in biological systems higher up the food chain [7–10,16,17]. Therefore, the most important aspects in addressing the potential problems caused by ^{99}Tc include (i) extraction of aqueous ^{99}TcO$_4^-$ from nuclear waste streams, which generally tend to be acidic solutions; (ii) high-efficiency selective removal of ^{99}TcO$_4^-$ at low concentrations from the contaminated water resources. However, it remains a huge challenge to develop sorbents capable of simultaneously realizing both these goals, owing to extreme conditions of high acidity, β decay by ^{99}Tc which can damage sorbents, adsorption competition with other anions, and the wide range of ^{99}TcO$_4^-$ concentrations found in nuclear wastes and contaminated water systems.

Traditional inorganic materials such as anion sodalite [18], layered double hydroxides [19–21], celluloses [22], silica [23–25], metal borates [26,27], and carbons [28,29] have all been explored as potential anion exchange adsorbents for ^{99}TcO$_4^-$ separation. Whilst some of these sorbents can initially remove ^{99}TcO$_4^-$ from aqueous acid solution at fast rates, they suffer in the longer term

* Corresponding authors.
  E-mail addresses: h.yang@ncepu.edu.cn (H. Yang), shengqian.ma@unt.edu (S. Ma), xkwang@ncepu.edu.cn (X. Wang).

from issues such as poor acid stability, poor radiation resistance, low $^{99}TcO_4^-$ adsorption capacity, and/or poor selectivity towards $^{99}TcO_4^-$ adsorption, thus limiting their practical applications. Amorphous porous organic polymers (POPs) demonstrate potential for selective anion adsorption, but buried anion sites resulting from disordered geometric pore structures often compromise their performance [30–36]. Metal−organic frameworks (MOFs) similarly offer promise for removing the $^{99}TcO_4^-$ from aqueous solutions, but maintaining structural integrity and initial adsorption performance is difficult under acidic conditions [37–46].

Recently, covalent organic frameworks (COFs) have emerged as a vibrant new class of crystalline porous materials, being well-suited to heavy metal ion decontamination due to their chemical inertness, periodic structures, and well-defined/tunable nanopores [47–62]. In a notable recent contribution, a cationic COF (SCU-COF-1) was developed for the selective adsorption of $^{99}TcO_4^-$ (and its non-radioactive analogue ReO_4^-). Owing to the limited availability and rarity of the purified radioactive $^{99}TcO_4^-$, ReO_4^- with identical charge density and similar anion exchange properties is commonly used as a $^{99}TcO_4^-$ surrogate [14]. To our knowledge, SCU-COF-1 is one of the few cationic COF-based sorbents developed to date for $^{99}TcO_4^-$ and ReO_4^- separation [61]. However, the Brunauer-Emmett-Teller (BET) surface area of SCU-COF-1 was only 22.98 $m^2 \, g^{-1}$, thus limiting the availability of anion exchange sites for $^{99}TcO_4^-$ or ReO_4^- adsorption (resulting in a low adsorption capacity). Most reported COFs are neutral frameworks [47–53,55–57,59–61,63]. Unlike neutral structures, the synthesis of cationic COFs for targeted anionic radionuclide remediation demands charged linkers. Constructing cationic COFs with well-defined architectures (accurate porosity) and high specific surface areas has proved technically challenging to date.

As a step-change advancement in the design of cationic COFs, we report herein a cationic 2D pyridinium salt-based COF (PS-COF-1), which exhibits large porosity and high surface area (2703 $m^2 \, g^{-1}$), good chemical stability, and excellent radiation resistance. We selected pyridinium salt linkers since they bind two chloride anions per molecular unit for charge balance, which we hypothesized could be replaced by $^{99}TcO_4^-$ (or its surrogate ReO_4^-) through the anion exchange processes. Structural characterization studies showed the COF adopted an eclipsed AA stacking structure with a pore size of ∼4.5 nm. When used as a sorbent for $ReO_4^-/^{99}TcO_4^-$, PS-COF-1 exhibited outstanding adsorption performance, delivering an uptake capacity of 1262 and 1180 mg g^{-1} at pH 6 and 3, respectively. Moreover, PS-COF-1 also exhibits excellent $ReO_4^-/^{99}TcO_4^-$ adsorption performance with a high uptake capacity and selectivity in the presence of large amounts of Cl^-, NO_3^-, SO_4^{2-}, Ac^-, $H_2PO_4^-$, Br^-, and CO_3^{2-} anions. Further, PS-COF-1 is able to reduce $ReO_4^-/^{99}TcO_4^-$ polluted potable water (∼10 ppb (part per billion), 100 ppb, or 1 ppm (part per million)) to drinking water level (0 ppb) within 10 min. In comparison, an amorphous POP analogue showed inferior performance under similar conditions. With a view towards practical applications, PS-COF-1 was able to remove $^{99}TcO_4^-$ efficiently from a simulated Hanford low-activity waste (LAW) stream, comparable to those found at US legacy nuclear sites. These results demonstrate that our studies offer valuable new insights for the rational design of sorbents for the extraction and separation of $^{99}TcO_4^-$ (and similar low charge density anions like ReO_4^-) from nuclear waste and polluted water.

2. Experimental

2.1. Synthesis of PS-COF-1

In a 5 mL glass tube, 1,3,5-tris(4-aminophenyl)benzene (TAPB, 28.1 mg) and 4,4′-bipyridinium, 1,1′-bis(4-formylphenyl) (Bpys, 52.5 mg) were dissolved in 1.1 mL of a solvent mixture of mesity-lene/ethanol (EtOH)/acetic acid (AcOH, 6 mol L^{-1}) in a 5:5:1 volume ratio. The mixture was then frozen in a liquid nitrogen bath, and sealed with a gas torch. After being heated at 80 °C for 72 h, the product was washed several times with THF and acetone, collected by filtration, and finally dried under vacuum overnight.

2.2. Synthesis of PS-Polymer-1

In a 5 mL glass tube, TAPB (28.1 mg) and 4,4′-bipyridinium, Bpys (52.5 mg) were dissolved in 1.1 mL of a solvent mixture of mesitylene/acetic acid (6 mol L^{-1}) in a volume ratio of 10:1. The mixture was then frozen in a liquid nitrogen bath, drained, and sealed with a gas torch. After being heated at 80 °C for 72 h, the product was washed several times with THF and acetone, collected by filtration, and finally dried under vacuum overnight.

2.3. Analysis of PS-COF-1

Fourier transform infrared spectroscopy (FTIR, Shimadzu high-resolution IRTracer-100), ^{13}C solid-state nuclear magnetic resonance spectroscopy (solid-state ^{13}C CP-MAS NMR, Bruker AVANCE III HD 600 MHz spectrometer), small angle X-ray scattering (SAXS, Rigaku SmartLab 9 K), and powder X-ray diffraction (PXRD, Rigaku SmartLab SE X-ray diffractometer equipped with a Cu Kα source) were used to determine the structure of PS-COF-1. Additional experimental and characterization details are included in the Supplementary materials (online).

3. Results

3.1. Synthesis and characterization of PS-COF-1

The synthetic strategy used to prepare PS-COF-1 is shown in Fig. 1. The FTIR spectrum of PS-COF-1 showed the disappearance of the –CHO and –NH₂ groups in the Bpys and TAPB precursors, respectively, whilst the appearance of a stretching vibration at 1677 cm^{-1} indicated the formation of C=N bonds (Fig. 2a). The solid-state ^{13}C CP-MAS NMR spectrum further showed a characteristic resonance signal at 161 ppm, confirming the presence of C=N bonds formed by the condensation reaction of aldehyde and amino groups in the starting materials (Fig. S1 online). The SAXS and PXRD patterns exhibited peaks at 1.7, 2.9, 3.4, and 25.3°, corresponding to the reflections from (100), (110), (200), and (001) planes (Fig. 2b and Fig. S2 online) of a two-dimensional (2D) layered COF. The Materials Studio software package was used to simulate the crystal structure [64]. After a geometrical energy minimization, Pawley refinement resulted in a hexagonal P6/m space group and unit cell parameters of $a = b = 59.36$ Å, $c = 3.52$ Å, $\alpha = \beta = 90°$, and $\gamma = 120°$, with $R_P = 0.37\%$ and $R_{WP} = 0.61\%$ (Tables S1 and S2 online). Compared to the possible eclipsed stacking (AA) or staggered stacking (AB) modes, the experimental data was a good match for the AA stacking mode. On the basis of these results, PS-COF-1 demonstrated a 2D structure with honeycomb-like pores with a theoretical dynamic pore size of 4.5 nm (Figs. 1 and 2c). The interlayer distance is approximately 3.6 Å. Scanning electron microscopy (SEM) revealed PS-COF-1 consisted of aggregated spherical particles (Fig. S3 online). Transmission electron microscopy (TEM) and high-resolution TEM (HRTEM) images revealed that the spherical particles were composed of stacked 2D sheets (Fig. S4 online). The lattice fringe spacing is around 3.7 Å, close to the calculated interlayer distance in the AA structure, confirming π–π stacking (Fig. S4c and d online). High-angle annular dark-field scanning transmission electron microscopy (HAADF-STEM) and corresponding elemental mapping images revealed the C, N, and Cl elements were uniformly distributed throughout the COF (Fig. 2d).
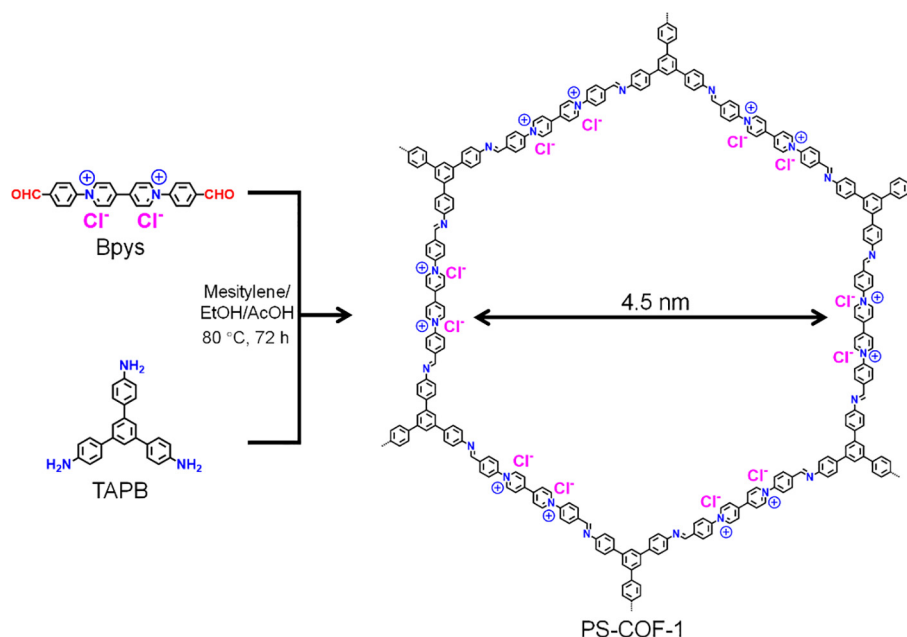
Fig. 1. Synthetic scheme of PS-COF-1 through the condensation of TAPB and Bpys.
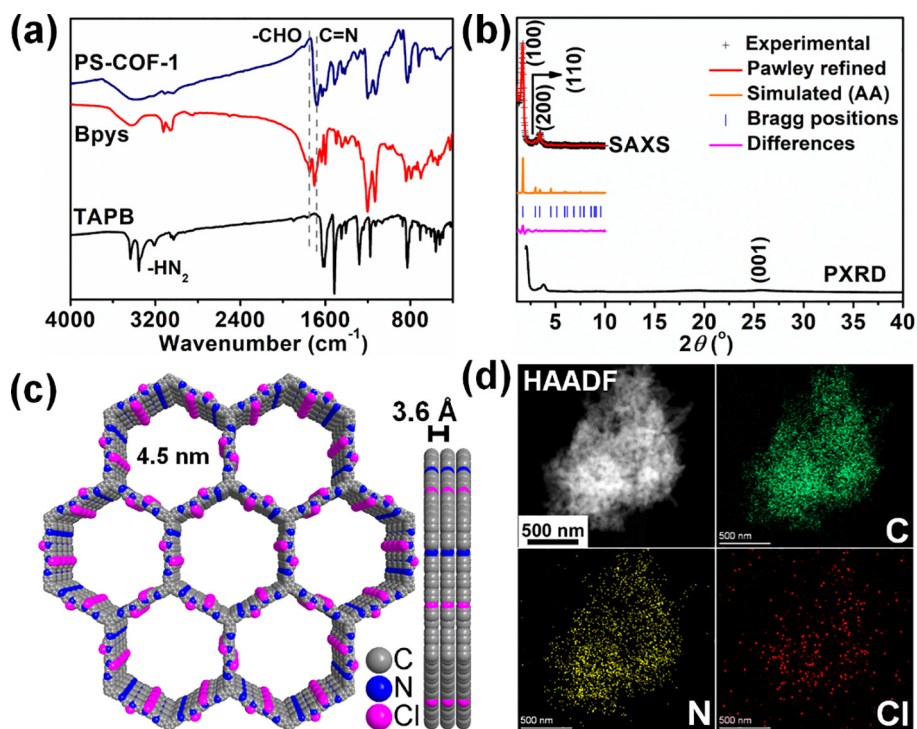
Fig. 2. Structural characterization of PS-COF-1. (a) FTIR spectra of PS-COF-1 together with TAPB and Bpys ligands. (b) Experimental and simulated SAXS (and PXRD) profiles of PS-COF-1. (c) Graphic view of the eclipsed AA stacking structure of PS-COF-1 (The C, N, and Cl atoms are represented by gray, blue, and magenta spheres in c). (d) HAADF-STEM and corresponding elemental mapping images to show the distributions of C (green), N (yellow), and Cl (red) in PS-COF-1.

3.2. Porosity and stability characterization

Thermogravimetric analysis (TGA) of PS-COF-1 revealed the structure was retained up to 430 °C, demonstrating the high stability of the COF (Fig. S5 online). The specific surface area and porosity of PS-CO-1 were determined by measuring N_2 adsorption–desorption isotherms at 77 K (Fig. 3a). The adsorption measurements showed a type IV isotherm, comprising sharp uptake at $P/P_0 < 0.12$, followed by a further steep increase in uptake at P/P_0 from 0.32–0.41, suggest-ing a narrow pore size distribution. The specific surface area was determined to be 2703 $m^2\,g^{-1}$, corresponding to a calculated micro-pore area and external surface area of 588 and 2115 $m^2\,g^{-1}$, respec-tively (Table S3 online). To the best of our knowledge, PS-COF-1 showed the highest experimental BET surface areas to date for any cationic COF [49,50]. The experimental total pore volume was deter-mined to be 2.68 $cm^3\,g^{-1}$ (Table S3 online). DFT pore size distribu-tion analysis showed mesopores with an average diameter of ~4.52 nm (Fig. S6 online), which agreed perfectly with the simulated
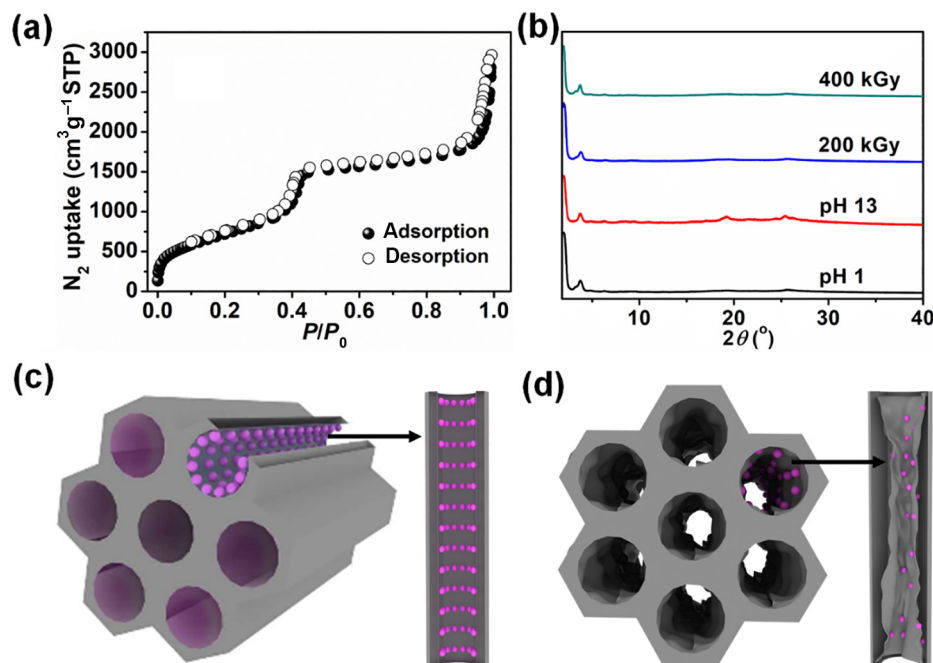
Fig. 3. Structural characterization of PS-COF-1, and schematic illustration of PS-COF-1 and PS-Polymer-1. (a) N_2 sorption isotherms measured at 77 K for PS-COF-1. (b) PXRD patterns of PS-COF-1 after treatments under various conditions. (c) Schematic illustration of PS-COF-1, showing abundant exposed Cl^- (pink spheres) within uniform pores. (d) Schematic illustration of PS-Polymer-1, showing partially collapsed pore channels and narrow bottlenecks. Due to the irregular pore diameters in PS-Polymer-1, many Cl^- sites were inaccessible to ReO_4^- and $^{99}TcO_4^-$, thus lowering the adsorption capacity for these anions.

crystallographic data. The high porosity of PS-COF-1 confirmed that the mesopores in the material were retained after removing the solvent molecules used in the COF's synthesis.

The chemical stability of PS-COF-1 was next studied by immersing the material into HNO_3 and NaOH aqueous solutions. The PXRD patterns showed the framework remained intact upon immersion in HNO_3 (pH 1) and NaOH (pH 13) solutions (Fig. 3b), indicating excellent chemical stability. To test the radiation resistance properties of PS-COF-1, the COF was subjected to γ-ray treatment. PXRD patterns indicate that the integrity of the framework was retained after 200 and 400 KGy γ-ray doses. Taken together, the excellent attributes of PS-COF-1 underscore its promise for applications such as $^{99}TcO_4^-$ extraction from radioactive wastes, which relies on sorbents with good physicochemical stability, high radiation resistance, and a high adsorption capacity through a porous structure.

The primary target of this research was the development of a high-performance cationic COF framework for anionic radionuclide remediation. As a control sorbent for PS-CO-1, an analogue sorbent PS-Polymer-1 was synthesized and characterized for further comparison (Fig. 3c and d). The syntheses of PS-COF-1 and PS-Polymer-1 were identical, except that the synthesis solvent was different (mesitylene/ethanol/acetic acid and mesitylene/acetic acid, respectively). FTIR and PXRD results revealed PS-Polymer-1 possessed an amorphous structure (Figs. S9 and S11 online). N_2 sorption measurements showed PS-Polymer-1 to have a BET surface area of 598 m^2 g^{-1} and pore volume of 0.69 cm^3 g^{-1}, respectively (Table S3, Figs. S7 and S8 online), both of which were much lower than PS-COF-1, suggesting a disordered structure with partially blocked pores.

3.3. ReO_4^- uptake properties

Based on the above results, we next conducted a series of experiments to assess the anionic radionuclide adsorption performance of PS-COF-1 and PS-Polymer-1. Because of the scarcity of purified radioactive $^{99}TcO_4^-$, the preliminary adsorption studies were conducted using ReO_4^- solutions ($^{99}TcO_4^-$ and ReO_4^- are very similar in terms of their structure, charge densities and water solubilities) [14]. The ReO_4^- adsorption abilities of PS-COF-1 were first examined at pH values ranging from 1 to 12 (Fig. 4a). A similar uptake capacity was obtained at pH values between 1 and 7, indicating the excellent adsorption properties of PS-COF-1 under acidic (HNO_3) and neutral conditions. PS-COF-1 offered lower adsorption capacities at high pH (10 to 12 range). Thus, PS-COF-1 is very well-suited to ReO_4^- (and thus $^{99}TcO_4^-$) extraction from acidic nuclear wastes and groundwater. As shown in Fig. 4b, PS-COF-1 could remove over 95.8% of ReO_4^- from dilute HNO_3 solutions (pH 6) at an adsorbent to liquid ratio of 50 mg L^{-1}, hence this dispersion concentration was used in subsequent studies. Equilibrium adsorption experiments were next conducted by varying the initial ReO_4^- concentrations from 0 to 800 ppm. After constant stirring over 15 h at 25 °C, the solutions were filtered, and the ReO_4^- concentrations in the filtrate quantified by UV-spectrophotometry. The adsorption capacity of PS-COF-1 was determined to be 1262 mg g^{-1} using a Langmuir model (calculated to be 1236 mg g^{-1}) (Fig. 4c, Tables S5 and S8 online). The detected pH of the solution decreased from 6 to 5.2 after the adsorption study. Kinetic studies verified that PS-COF-1 displayed fast ReO_4^- adsorption kinetics, with an adsorption equilibrium time of 180 min at pH 6 (Fig. 4d). In comparison, the PS-Polymer-1 sorbent showed a much lower ReO_4^- uptake capacity under the same conditions (Fig. 4e and f). This is likely due to many of the active sites (i.e., exchangeable Cl^- sites) being inaccessible, thereby detrimentally impacting adsorption performance (Fig. 3c and d). Adsorption capacities were next determined in pH 3 nitric acid solutions. Remarkably, a high ReO_4^- uptake capacity of 1180 mg g^{-1} was observed (Fig. 4g, h, and Table S7 online). The equilibrium adsorption data could again be well-fitted using a Langmuir isotherm model (calculated to be 1159 mg g^{-1}), with correlation coefficients >0.97 realized at pH 3 (c.f. >0.95 at pH 6) (Tables S5 and S7 online). The ReO_4^- adsorption ability of PS-COF-
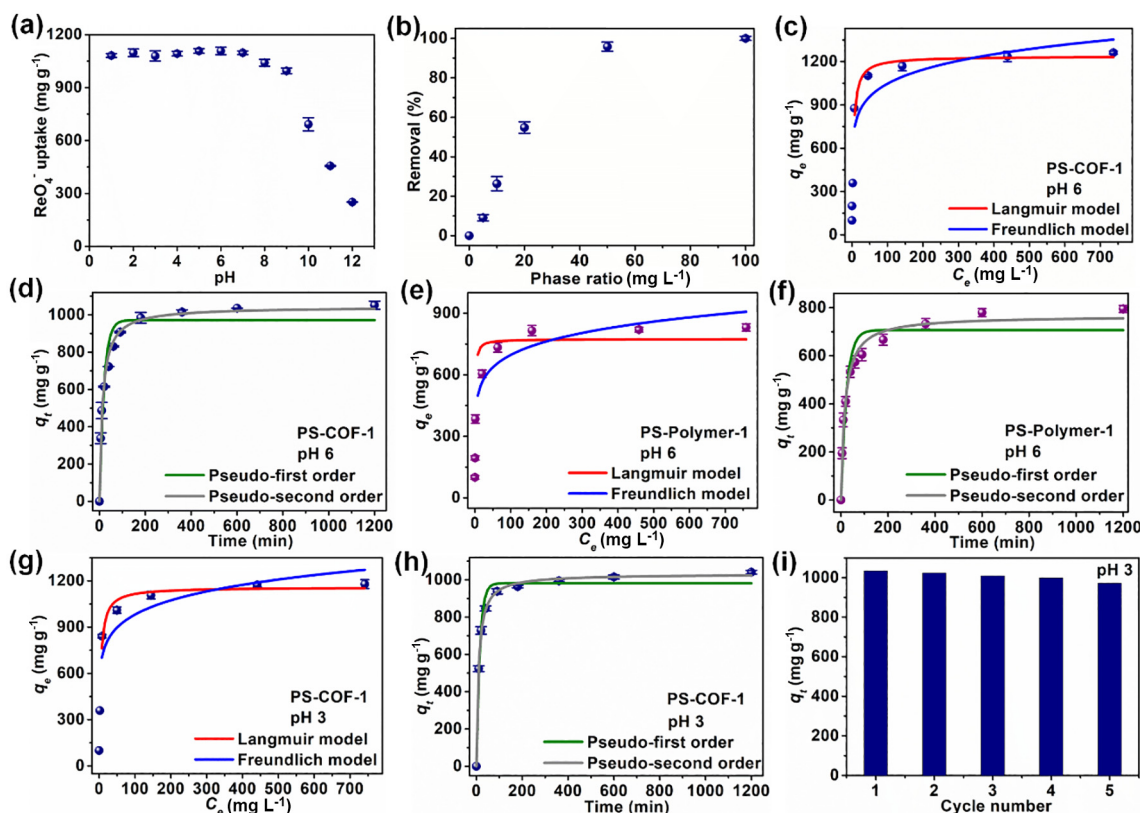
Fig. 4. ReO$_4^-$ adsorption results. (a) Effect of pH on the removal of ReO$_4^-$. (b) ReO$_4^-$ removal by PS-COF-1 at various adsorbent-liquid ratios. (c, e) Equilibrium adsorption isotherms for ReO$_4^-$ on PS-COF-1 and PS-Polymer-1 at pH 6, respectively. (d, f) ReO$_4^-$ adsorption kinetics on PS-COF-–1 and PS-Polymer-1 at an initial ReO$_4^-$ concentration of ~56 ppm (pH 6), respectively. (g, h) Equilibrium isotherms and adsorption kinetics of ReO$_4^-$ on PS-COF-1 at pH 3, respectively. (i) Recycle test data for ReO$_4^-$ removal in HNO$_3$ (at pH 3) solutions by PS-COF-1.

1 was on par or surpassed the best sorbents previously reported in the literature (Table S8 online). It is worth mentioning that PS-COF-1 can readily be regenerated by elution with a NaCl solution, with an adsorption capacity of 954 mg g^{-1} maintained over five cycles in pH 3 HNO$_3$ solution (Fig. 4i). The ReO$_4^-$ removal efficiency of PS-COF-1 was unchanged after six test cycles at pH 6 (Fig. S12 online). PXRD confirmed the crystallinity of PS-COF-1 was retained after the cycle tests, confirming good sorbent durability (Fig. S13 online).

Considering the coexistence of large excesses of competing anions in nuclear wastewater and contaminated water, such as NO$_3^-$, Cl$^-$, Ac$^-$, SO$_4^{2-}$, Br$^-$, and so on, the effects of these anions on the capture of ReO$_4^-$ (and by analogy ^{99}TcO$_4^-$) was explored. Notably, PS-COF-1 maintained an excellent ReO$_4^-$ uptake capacities in the presence of the various competing anions at pH 6 (Fig. 5a). As shown in Fig. 5b, the relative ReO$_4^-$ removal efficiency was 99%, 94%, and 81% at NO$_3^-$:ReO$_4^-$ molar ratios of 1:1, 1:100, and 1000:1, respectively. Further studies revealed PS-COF-1 also showed excellent selectivity for ReO$_4^-$ against other anions (such as Ac$^-$, CO$_3^{2-}$, SO$_4^{2-}$, Cl$^-$, and H$_2$PO$_4^-$) under high ionic strength conditions (Figs. S14–S18 online). In general, high charge density anions demonstrate stronger electrostatic interactions with adsorbents than low charge density anions. The adsorption results revealed that PS-COF-1 offered a strong affinity for ReO$_4^-$ and ^{99}TcO$_4^-$, even at high ionic strengths. This latter behavior was quite different to traditional anion exchange resins and MOFs, which tend to show a higher affinity for anions with lower charge densities at high ionic strengths [34,39,41,43].

Compared to acidic nuclear waste, radioactively contaminated potable water will generally contain a much lower concentration of nuclides. Thus, we carried out further adsorption experiments

at ReO$_4^-$ polluted potable water. PS-COF-1 demonstrated a fast ReO$_4^-$ uptake at low concentrations, reaching over 99.9% of their equilibrium adsorption capacity within 10 min in ~10, 100, and 1000 ppb ReO$_4^-$ solutions, respectively (Fig. 5c). The results highlight the outstanding properties of PS-COF-1 as a sorbent for the efficient and highly selective removal of ReO$_4^-$ (and ^{99}TcO$_4^-$) at low concentrations from contaminated water resources.

3.4. ^{99}TcO$_4^-$ uptake properties

Encouraged by the ReO$_4^-$ adsorption studies, we then performed ^{99}TcO$_4^-$ adsorption studies to validate the adsorption performance of PS-COF-1. In a ~14 ppm ^{99}TcO$_4^-$ solution, the removal efficiency reached >97.8% in 20 min (>99% in 60 min, comparable to other reported materials, Table S9 online) (Fig. 5d). As expected, the test results were remarkably consistent with those of the ReO$_4^-$ adsorption studies, encouraging the potential use of PS-COF-1 for the efficient removal of ^{99}TcO$_4^-$ from nuclear waste and contaminated water. Removing TcO$_4^-$ from Hanford low-activity waste (LAW) melter recycle streams at US legacy nuclear sites is challenging, though industrially relevant for nuclear waste remediation [16,30,65]. In this context, we set about exploring the adsorption properties of the PS-COF-1 under conditions relevant to LAW waste solutions. LAW streams have a high ionic strength containing large amounts of SO$_4^{2-}$, NO$_3^-$, NO$_2^-$, Cl$^-$, and CO$_3^{2-}$, with total anions concentrations more than thousand times that of ^{99}TcO$_4^-$ (Table S10 online). Attractively, the removal efficiency of ^{99}TcO$_4^-$ was >75.3% in 2 h under conditions relevant Hanford LAW streams (at a PS-COF-1 to solution ratio of 5 mg mL^{-1}). We further estimated the cost of synthesizing PS-COF-1 to be ~$64.5 USD g^{-1}, suggesting its economic feasibility for nuclear waste management. These
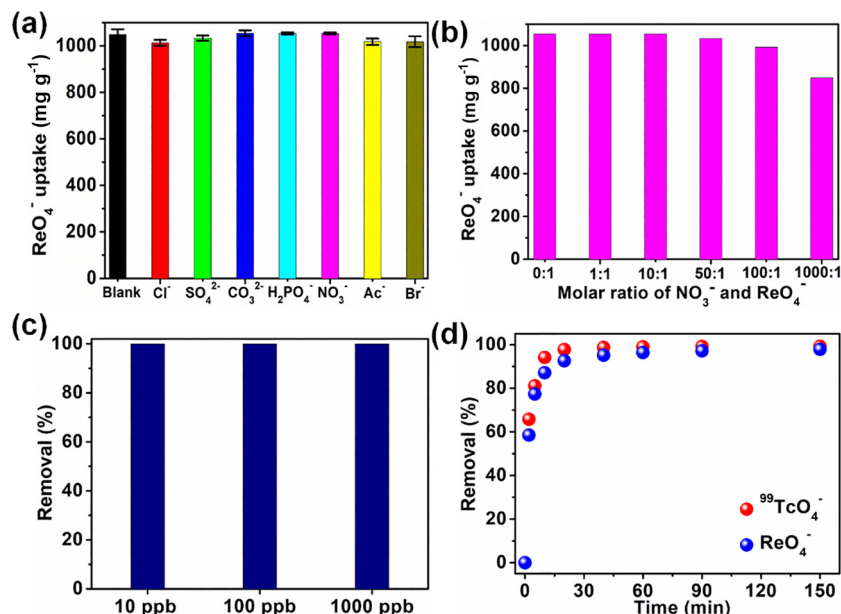
Fig. 5. ReO_4^- and $^{99}TcO_4^-$ adsorption performance of PS-COF-1. (a) Effect of possible competing anions on ReO_4^- uptake by PS-COF-1 via anion exchange. (b) Effect of different concentrations of NO_3^- on the anion exchange of ReO_4^- by PS-COF-1 in ~10, 100, and 1000 ppb ReO_4^- solutions containing possible competing anions. (c) Removal efficiency (after 10 min) of ReO_4^- by PS-COF-1 in ~10, 100 and 1000 ppb ReO_4^- solutions containing possible competing anions. (d) $^{99}TcO_4^-$ and ReO_4^- adsorption kinetics on PS-COF-1 at an initial $^{99}TcO_4^-$ and ReO_4^- concentration of ~14 and ~28 ppm, respectively. Caution: $^{99}TcO_4^-$ may lead to radiation hazards. Therefore, the $^{99}TcO_4^-$ adsorption studies were carried out in a licensed laboratory dedicated to radiological investigations.

results indicate that PS-COF-1 could indeed be very useful for removing $^{99}TcO_4^-$ efficiently from high ionic strength Hanford LAW inventories.

3.5. Distinctive adsorption mechanism

After demonstrating the excellent perrhenate and pertechnetate extraction performance of PS-COF-1 in acidic and near-neutral solutions, we sought to better understand the adsorption mechanism by carrying out FTIR, HAADF-STEM/elemental mapping, X-ray photoelectron spectroscopy (XPS), solid-state ^{13}C CP/MAS NMR measurements, and DFT calculations. The FTIR spectrum of the used PS-COF-1 sorbent revealed the appearance of a v_3 Re–O asymmetric stretch at 910 cm^{-1} after the adsorption experiments (Fig. 6a). HAADF-STEM/corresponding elemental mapping images and XPS of the used sorbent showed the presence of Re signals together with the complete disappearance of chloride, indicating the saturation adsorption of ReO_4^- by ion exchange (Figs. S19–S21 online). The solid-state ^{13}C CP/MAS NMR spectrum further showed the structure of PS-COF-1 was retained, which indicated that strong interactions between ReO_4^- and pyridine N(+) sites did not affect the skeleton structure of the material (Fig. 6b). Next, we performed DFT calculations [66–68]. Since the anion exchange processes will take place at the positively charged pyridine N(+) sites, we considered the possible affinity contributions from all surrounding atoms. The structural models of An^-/M^+ (An^- = Cl$^-$, NO_3^-, HSO_4^-, $^{99}TcO_4^-$; M^+ = two layers of pyridine ring units) were chosen to represent the 2D layered structure of PS-COF-1. Fig. 6c shows the model of $^{99}TcO_4^-$/PS-COF-1. The Stuttgart/Dresden (SDD) basis set was used for Tc atoms, and 6-311+G(d,p) was employed for other atoms for geometry optimization before performing calculations [67,69,70]. The solvent effect of water was examined using the self-consistent reaction field (SCRF) method based on SMD solvent model [68]. Subsequently, the binding free energies (potential of mean force, ΔE) of PS-COF-1 with NO_3^-, Cl$^-$, HSO_4^-, and $^{99}TcO_4^-$ were calculated and compared. As shown in Fig. 6d, the calculated binding free energy of $^{99}TcO_4^-$/PS-COF-1

was −0.424 eV. In comparison, the calculated energies for Cl$^-$/PS-COF-1, NO_3^-/PS-COF-1, and HSO_4^-/PS-COF-1 (HSO_4^- was used to replace SO_4^{2-} for equal valence comparison) were −0.298, −0.361, and −0.305 eV, respectively, all lower than $^{99}TcO_4^-$/PS-COF-1 (absolute value). The calculations suggest that ion exchange will follow the trend $^{99}TcO_4^- > NO_3^- > HSO_4^- > Cl^-$ (i.e. $^{99}TcO_4^-$ will readily replace adsorbed Cl$^-$ readily on the pyridine N(+) sites). The theoretical calculations are thus in excellent accord with the experimental findings, further confirming the efficient and selective $^{99}TcO_4^-$/ReO_4^- adsorption properties of PS-COF-1. The high selectivity towards $^{99}TcO_4^-$ and ReO_4^- adsorption can be ascribed to the strong electrostatic interaction between these low charge density anions and the hydrophobic cationic pore structure of PS-COF-1 [27,34].

4. Discussion and conclusion

Considering the aforementioned findings, it can be concluded that PS-COF-1 is an excellent sorbent for $^{99}TcO_4^-$ and ReO_4^- under wide ranging conditions of pH, $^{99}TcO_4^-$/ReO_4^- concentration, and ionic strength, even in the presence of high concentrations of other anions. The remarkable selective adsorption performance of this material can be attributed to: (i) the good physicochemical stability and radiation resistance of the COF, which allowed adsorption studies under extreme conditions; (ii) the eclipsed AA stacking structure of the COF with large honeycomb-like pores and super high surface area, facilitating facile access of $^{99}TcO_4^-$ and ReO_4^- to accessible pyridine N(+) sorption sites; (iii) the pyridine linkers in the crystalline structure offered abundant cationic sites with relatively low affinity for anions other than $^{99}TcO_4^-$ and ReO_4^- in acidic and neutral solutions; (iv) the surrounding atoms close to pyridine N(+) sites in the framework which acted cooperatively to ensure strong affinities for $^{99}TcO_4^-$ and ReO_4^- during the adsorption process. These results will encourage the future development of other cationic pyridinium salt-based COFs as novel porous sorbents for selective anion removal from nuclear wastes and other contaminated water sources.
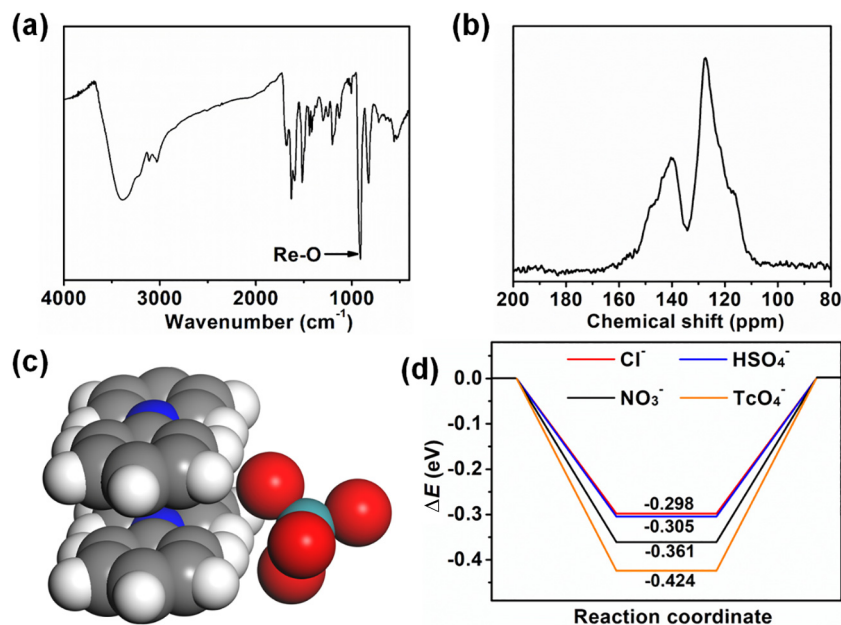
Fig. 6. Identification of the adsorption mechanism. (a) FTIR spectrum of PS-COF-1 after ReO_4^- adsorption. (b) Solid-state ^{13}C CP/MAS NMR spectrum of PS-COF-1 after ReO_4^- adsorption. (c) Structural model of $^{99}TcO_4^-$/PS-COF-1 (C, gray; N, blue; O, red; H, white; and Tc, dark cyan). (d) Binding free energies (ΔE) of PS-COF-1 to different anions determined by DFT calculations.

In conclusion, a cationic covalent organic framework PS-COF-1 was successfully constructed using a pyridinium salt-based linker. Benefitting from extraordinary surface area and ordered porosity, physicochemical, and radiation stability, PS-COF-1 exhibited excellent ReO_4^- and $^{99}TcO_4^-$ selective capture abilities in the presence of large excesses of other anions under acidic/neutral conditions. PS-COF-1 achieved a 100% ReO_4^- and $^{99}TcO_4^-$ uptake capacity at low concentrations (<1 ppm) in contaminated water. DFT calculations revealed that pore environments around cationic pyridine N(+) sites in the COF framework showed a high affinity for ReO_4^- and $^{99}TcO_4^-$, hence explaining the high adsorption selectivity for these anions. This study conclusively demonstrates that pyridinium salt-based COF materials have enormous potential for the separation of $^{99}TcO_4^-$ from nuclear waste, contaminated water, and environmental remediation.

Conflict of interest

The authors declare that they have no conflict of interest.

Author contributions

Hui Yang, Xiangke Wang, and Shengqian Ma conceived and designed the research. Mengjie Hao and Zhongshan Chen performed the synthesis and characterization. Mengjie Hao and Zhongshan Chen carried out the adsorption tests. Hui Yang, Xiangke Wang, Geoffrey I. N. Waterhouse, and Shengqian Ma wrote the manuscript. All authors contributed to the discussion, and gave approval to the final version of the manuscript.

Appendix A. Supplementary materials

Supplementary materials to this article can be found online at https://doi.org/10.1016/j.scib.2022.02.012.

References

[1] Adamantiades A, Kessides I. Nuclear power for sustainable development: current status and future prospects. Energy Policy 2009;37:5149–66.
[2] Mayer K, Wallenius M, Lutzenkirchen K, et al. Uranium from german nuclear power projects of the 1940s—a nuclear forensic investigation. Angew Chem Int Ed 2015;54:13452–6.
[3] Dresselhaus MS, Thomas IL. Alternative energy technologies. Nature 2001;414:332–7.
[4] Banerjee D, Kim D, Schweiger MJ, et al. Removal of TcO_4^- ions from solution: materials and future outlook. Chem Soc Rev 2016;45:2724–39.
[5] Taylor R. Reaction: a role for actinide chemists. Chem 2016;1:662–3.
[6] Lee MS, Um W, Wang G, et al. Impeding ^{99}Tc(IV) mobility in novel waste forms. Nat Commun 2016;7:12067.
[7] del Cul GD, Bostick WD, Trotter DR, et al. Technetium-99 removal from process solutions and contaminated groundwater. Sep Sci Technol 1993;28:551–64.
[8] Amendola V, Bergamaschi G, Boiocchi M, et al. Fluorescent sensing of ^{99}Tc pertechnetate in water. Chem Sci 2014;5:1820–6.
[9] Seliman AF, Samadi A, Husson SM, et al. Preparation of polymer-coated, scintillating ion-exchange resins for monitoring of ^{99}Tc in groundwater. Anal Chem 2011;83:4759–66.
[10] Eagling J, Worsfold PJ, Blake WH, et al. Mobilization of technetium from reduced sediments under seawater inundation and intrusion scenarios. Environ Sci Technol 2012;46:11798–803.
[11] Wilmarth WR, Lumetta GJ, Johnson ME, et al. Review: waste-pretreatment technologies for remediation of legacy defense nuclear wastes. Solvent Extr Ion Exch 2011;29:1–48.
[12] Murphy CE, Johnson TL. Vegetative uptake of technetium-99 from buried, solidified, low-level radioactive waste. J Environ Qual 1993;22:793–9.
[13] Xiao C, Khayambashi A, Wang S. Separation and remediation of $^{99}TcO_4^-$ from aqueous solutions. Chem Mater 2019;31:3863–77.
[14] Darab JG, Smith PA. Chemistry of technetium and rhenium species during low-level radioactive waste vitrification. Chem Mater 1996;8:1004–21.
[15] Icenhower JP, Qafoku NP, Zachara JM, et al. The biogeochemistry of technetium: a review of the behavior of an artificial element in the natural environment. Am J Sci 2011;310:721–52.

[16] King WD, Hassan NM, McCabe DJ, et al. Technetium removal from hanford and savannah river site actual tank waste supernates with superlig® 639 resin. Sep Sci Technol 2003;38:3093–114.

[17] DiPrete DP, DiPrete CC, Sigg RA. Measurement of ^{99}Tc in savannah river site high activity waste. J Radioanal Nucl Chem 2005;263:593–8.

[18] Dickson JO, Harsh JB, Flury M, et al. Competitive incorporation of perrhenate and nitrate into sodalite. Environ Sci Technol 2014;48:12851–7.

[19] Wang Y, Gao H. Compositional and structural control on anion sorption capability of layered double hydroxides (LDHs). J Colloid Interface Sci 2006;301:19–26.

[20] Fei H, Bresler MR, Oliver SR. A new paradigm for anion trapping in high capacity and selectivity: crystal-to-crystal transformation of cationic materials. J Am Chem Soc 2011;133:11110–3.

[21] Sheng G, Tang Y, Linghu W, et al. Enhanced immobilization of ReO$_4^-$ by nanoscale zerovalent iron supported on layered double hydroxide via an advanced xafs approach: implications for TcO$_4^-$ sequestration. Appl Catal B Environ 2016;192:268–76.

[22] Wen D, Hua R, Dong Z, et al. Efficient separation and recovery of Re(VII) from Re/U bearing acidic solutions using aminotriazole modified cellulose microsphere adsorbents. Environ Sci Pollut Res Int 2021;28:52225–35.

[23] Weng H, Zhang P, Guo Z, et al. Efficient and ultrafast adsorption of rhenium by functionalized hierarchically mesoporous silica: a combined strategy of topological construction and chemical modification. ACS Appl Mater Interfaces 2021;13:8249–62.

[24] Shan W, Zhang Y, Shu Y, et al. Enhanced adsorption and separation of Re(VII) using organic-inorganic hybrid silica adsorbent. Microporous Mesoporous Mater 2021;317:110980.

[25] Shan W, Wang D, Zhang Z, et al. Synthesis of Schiff base-functionalized silica for effective adsorption of Re(VII) from aqueous solution. J Taiwan Inst Chem Eng 2019;100:277–84.

[26] Wang S, Alekseev EV, Diwu J, et al. NDTB-1: a supertetrahedral cationic framework that removes TcO$_4^-$ from solution. Angew Chem Int Ed 2010;49:1057–60.

[27] Wang S, Yu P, Purse BA, et al. Selectivity, kinetics, and efficiency of reversible anion exchange with TcO$_4^-$ in a supertetrahedral cationic framework. Adv Funct Mater 2012;22:2241–50.

[28] Xiong Y, Cui X, Zhang P, et al. Improving Re(VII) adsorption on diisobutylamine-functionalized graphene oxide. ACS Sustain Chem Eng 2016;5:1010–8.

[29] Gao Y, Chen K, Tan X, et al. Interaction mechanism of Re(VII) with zirconium dioxide nanoparticles archored onto reduced graphene oxides. ACS Sustain Chem Eng 2017;5:2163–71.

[30] Sun Q, Zhu L, Aguila B, et al. Optimizing radionuclide sequestration in anion nanotraps with record pertechnetate sorption. Nat Commun 2019;10:1646.

[31] Li X, Li Y, Wang H, et al. 3D cationic polymeric network nanotrap for efficient collection of perrhenate anion from wastewater. Small 2021;17:2007994.

[32] Samanta P, Chandra P, Dutta S, et al. Chemically stable ionic viologen-organic network: an efficient scavenger of toxic oxo-anions from water. Chem Sci 2018;9:7874–81.

[33] Li J, Dai X, Zhu L, et al. ^{99}TcO$_4^-$ remediation by a cationic polymeric network. Nat Commun 2018;9:3007.

[34] Zhu L, Xiao C, Dai X, et al. Exceptional perrhenate/pertechnetate uptake and subsequent immobilization by a low-dimensional cationic coordination polymer: overcoming the hofmeister bias selectivity. Environ Sci Technol Lett 2017;4:316–22.

[35] Li J, Chen L, Shen N, et al. Rational design of a cationic polymer network towards record high uptake of ^{99}TcO$_4^-$ in nuclear waste. Sci China Chem 2021;64:1251–60.

[36] Li J, Li B, Shen N, et al. Task-specific tailored cationic polymeric network with high base-resistance for unprecedented ^{99}TcO$_4^-$ cleanup from alkaline nuclear waste. ACS Cent Sci 2021;7:1441–50.

[37] Sheng D, Zhu L, Dai X, et al. Successful decontamination of ^{99}TcO$_4^-$ in groundwater at legacy nuclear sites by a cationic metal−organic framework with hydrophobic pockets. Angew Chem Int Ed 2019;58:4968–72.

[38] Drout RJ, Otake K, Howarth AJ, et al. Efficient capture of perrhenate and pertechnetate by a mesoporous Zr metal−organic framework and examination of anion binding motifs. Chem Mater 2018;30:1277–84.

[39] Sheng D, Zhu L, Xu C, et al. Efficient and selective uptake of TcO$_4^-$ by a cationic metal−organic framework material with open Ag$^+$ sites. Environ Sci Technol 2017;51:3471–9.

[40] Li J, Wang X, Zhao G, et al. Metal−organic framework-based materials: superior adsorbents for the capture of toxic and radioactive metal ions. Chem Soc Rev 2018;47:2322–56.

[41] Zhu L, Sheng D, Xu C, et al. Identifying the recognition site for selective trapping of ^{99}TcO$_4^-$ in a hydrolytically stable and radiation resistant cationic metal−organic framework. J Am Chem Soc 2017;139:14873–6.

[42] Zhang D, Ronson TK, Mosquera J, et al. Selective anion extraction and recovery using a Fe$_4^{(II)}$L$_4$ cage. Angew Chem Int Ed 2018;57:3717–21.

[43] Banerjee D, Xu W, Nie Z, et al. Zirconium-based metal−organic framework for removal of perrhenate from water. Inorg Chem 2016;55:8241–3.

[44] Kang K, Dai X, Shen N, et al. Unveiling the uncommon fluorescent recognition mechanism towards pertechnetate using a cationic metal−organic framework bearing n-heterocyclic aie molecules. Chem Eur J 2021;27:5632–7.

[45] Kang K, Li L, Zhang M, et al. Constructing cationic metal−organic framework materials based on pyrimidyl as a functional group for perrhenate/pertechnetate sorption. Inorg Chem 2021;60:16420–8.

[46] Kang K, Shen N, Wang Y, et al. Efficient sequestration of radioactive ^{99}TcO$_4^-$ by a rare 3-fold interlocking cationic metal−organic framework: a combined batch experiments, pair distribution function, and crystallographic investigation. Chem Eng J 2022;427:130942.

[47] Chen X, Geng K, Liu R, et al. Covalent organic frameworks: chemical approaches to designer structures and built-in functions. Angew Chem Int Ed 2020;59:5050–91.

[48] Li Y, Chen W, Xing G, et al. New synthetic strategies toward covalent organic frameworks. Chem Soc Rev 2020;49:2852–68.

[49] Wang Z, Zhang S, Chen Y, et al. Covalent organic frameworks for separation applications. Chem Soc Rev 2020;49:708–35.

[50] Song Y, Sun Q, Aguila B, et al. Opportunities of covalent organic frameworks for advanced applications. Adv Sci 2019;6:1801410.

[51] Yahiaoui O, Fitch AN, Hoffmann F, et al. 3D anionic silicate covalent organic framework with srs topology. J Am Chem Soc 2018;140:5330–3.

[52] Lohse MS, Bein T. Covalent organic frameworks: structures, synthesis, and applications. Adv Funct Mater 2018;28:1705553.

[53] Mitra S, Kandambeth S, Biswal BP, et al. Self-exfoliated guanidinium-based ionic covalent organic nanosheets (iCONs). J Am Chem Soc 2016;138:2823–8.

[54] Yu S-B, Lyu H, Tian J, et al. A polycationic covalent organic framework: a robust adsorbent for anionic dye pollutants. Polym Chem 2016;7:3392–7.

[55] Zhang Y, Duan J, Ma D, et al. Three-dimensional anionic cyclodextrin-based covalent organic frameworks. Angew Chem Int Ed 2017;56:16313–7.

[56] Mal A, Mishra RK, Praveen VK, et al. Supramolecular reassembly of self-exfoliated ionic covalent organic nanosheets for label-free detection of double-stranded DNA. Angew Chem Int Ed 2018;57:8443–7.

[57] Du Y, Yang H, Whiteley JM, et al. Ionic covalent organic frameworks with spiroborate linkage. Angew Chem Int Ed 2016;55:1737–41.

[58] Wang Y, Xie M, Lan J, et al. Radiation controllable synthesis of robust covalent organic framework conjugates for efficient dynamic column extraction of ^{99}TcO$_4^-$. Chem 2020;6:2796–809.

[59] Li Z, Li H, Guan X, et al. Three-dimensional ionic covalent organic frameworks for rapid, reversible, and selective ion exchange. J Am Chem Soc 2017;139:17771–4.

[60] Lu Q, Ma Y, Li H, et al. Postsynthetic functionalization of three-dimensional covalent organic frameworks for selective extraction of lanthanide ions. Angew Chem Int Ed 2018;57:6042–8.

[61] He L, Liu S, Chen L, et al. Mechanism unravelling for ultrafast and selective ^{99}TcO$_4^-$ uptake by a radiation-resistant cationic covalent organic framework: a combined radiological experiment and molecular dynamics simulation study. Chem Sci 2019;10:4293–305.

[62] Mollick S, Fajal S, Saurabh S, et al. Nanotrap grafted anion exchangeable hybrid materials for efficient removal of toxic oxoanions from water. ACS Cent Sci 2020;6:1534–41.

[63] Cheng G, Zhang A, Zhao Z, et al. Extremely stable amidoxime functionalized covalent organic frameworks for uranium extraction from seawater with high efficiency and selectivity. Sci Bull 2021;66:1996–2001.

[64] Akkermans RLC, Spenley NA, Robertson SH. Monte carlo methods in materials studio. Mol Simul 2013;39:1153–64.

[65] Shen N, Yang Z, Liu S, et al. ^{99}TcO$_4^-$ removal from legacy defense nuclear waste by an alkaline-stable 2D cationic metal organic framework. Nat Commun 2020;11:5571.

[66] Zhao Y, Truhlar DG. The M06 suite of density functionals for main group thermochemistry, thermochemical kinetics, noncovalent interactions, excited states, and transition elements: two new functionals and systematic testing of four M06-class functionals and 12 other functionals. Theor Chem Acc 2007;120:215–41.

[67] Grimme S, Ehrlich S, Goerigk L. Effect of the damping function in dispersion corrected density functional theory. J Comput Chem 2011;32:1456–65.

[68] Marenich AV, Cramer CJ, Truhlar DG. Universal solvation model based on solute electron density and on a continuum model of the solvent defined by the bulk dielectric constant and atomic surface tensions. J Phys Chem B 2009;113:6378–96.

[69] Hehre WJ, Ditchfield R, Pople JA. Self-consistent molecular orbital methods. XII. Further extensions of gaussian-type basis sets for use in molecular orbital studies of organic molecules. J Chem Phys 1972;56:2257–61.

[70] Hariharan PC, Pople JA. The influence of polarization functions on molecular orbital hydrogenation energies. Theoret Chim Acta 1973;28:213–22.

Mengjie Hao received her B.S. degree from North China Electric Power University in 2020. Now she is a Ph.D. candidate at the College of Environmental Science and Engineering, North China Electric Power University. Her research focuses on the design and synthesis of highly efficient covalent organic framework (COF) material for environmental management.

Hui Yang earned his Ph.D. degree in 2013 from Northwestern Polytechnical University. After finishing his research experiences at National Institute of Advanced Industrial Science and Technology, Massey University, and the University of South Florida, he started to serve as an associate professor at North China Electric Power University. His current research interest is the synthesis and application of porous materials for energy, radioactive, and environmental-related applications.

Xiangke Wang is a full professor of the College of Environmental Science and Engineering, North China Electric Power University. He received his B.S. degree in 1995 and Ph.D. degree in 2000 from Lanzhou University. Then he joined the SUBATECH Laboratory (France) as a research fellow and the Karlsruhe Research Center (Germany) as Alexander von Humboldt research fellow. He focuses on the synthesis of nanomaterials and their applications in energy and environmental pollution management, and also the characterization of radionuclide physicochemical behaviour in the environment.

Shengqian Ma obtained his B.S. degree from Jilin University in 2003, and graduated from Miami University (Ohio) with a Ph.D. degree in 2008. After a two-year Director's Postdoctoral Fellowship at Argonne National Laboratory, he joined the Department of Chemistry at the University of South Florida (USF) as an assistant professor in 2010. He was promoted to an associate professor with early tenure in 2015 and to a full professor in 2018. In 2020, he joined the Department of Chemistry at University of North Texas (UNT) as the Robert A. Welch Chair in Chemistry. His current research interest focuses on task-specific design and functionalization of advanced porous materials for energy, biological, and environmental-related applications.